CMS Physics Analysis Summary

Contact: cms-pag-conveners-b2g@cern.ch 2015/03/11

A search for resonant $t\bar{t}$ production in all final states in pp collisions at $\sqrt{s} = 8$ TeV

The CMS Collaboration

Abstract

A search is presented for the production of heavy resonances decaying into top-antitop quark pairs in events with three different final states, defined by the number of leptons from the $t\bar{t} \to WbWb$ decay. The data correspond to an integrated luminosity of 19.7 fb^{-1} and was collected by the CMS detector in proton-proton collisions at $\sqrt{s} = 8$ TeV. The selections are optimized for reconstruction of top quarks with high Lorentz boosts, where jet substructure techniques are used to enhance the sensitivity. No significant excess of events over the expected yield from standard model processes is observed. Upper limits on the production cross section of heavy resonances decaying to $t\bar{t}$ are calculated using all channels. A narrow leptophobic topcolor Z' resonance with a mass below 2.4 TeV is excluded at a 95% confidence level. Limits are also derived for a broad Z' resonance with 10% width and a Kaluza-Klein excitation of the gluon in the Randall-Sundrum model.

1 Introduction

The top quark is the heaviest known fundamental particle with a mass close to the electroweak scale. As such, it has a strong Yukawa coupling to the Higgs potential and is therefore closely connected to the hierarchy problem, where the largest corrections to the mass of the Higgs boson arise from top-quark loops. Studies of top-quark production may provide further insight into the mechanism of electroweak symmetry breaking, especially in the light of the recent discovery of the Higgs boson and the measurement of its mass [1–3].

Many theories beyond the standard model (SM) predict the existence of heavy resonances, generically referred to as Z', that preferentially decay to $t\bar{t}$ pairs and manifest themselves as a resonant component in addition to the SM $t\bar{t}$ continuum production. Examples of such models include colorons [4–7], extended gauge theories with massive color-singlet Z-like bosons [8–10], axigluons [11, 12] and models in which a pseudoscalar Higgs boson may couple strongly to top quarks [13]. Furthermore, various extensions of the Randall–Sundrum model [14] with extra dimensions predict Kaluza–Klein (KK) excitations of gluons g_{KK} [15] or gravitons [16], both of which can have enhanced couplings to $t\bar{t}$ pairs. Direct searches for heavy $t\bar{t}$ resonances have been performed at the CERN LHC collider, with results consistent with the SM and sub-picobarn limits on the production cross section in the mass range of 1-3 TeV [17–22].

This document presents a model independent search for $Z' \to t\bar{t} \to W^+bW^-\bar{b}$ production[1], where the leptonic and hadronic decay modes of the W bosons are considered. This results in final states with two, one, or zero leptons (electron or muon), that are referred to as the dilepton, lepton+jets, and all-hadronic channels, respectively. The search is based on pp collision data collected by CMS at $\sqrt{s} = 8\,\text{TeV}$, corresponding to an integrated luminosity of $19.7\,\text{fb}^{-1}$. The combination of the three possible final states, together with improvements due to the use of jet substructure techniques and b tagging in collimated topologies, results in a much higher sensitivity than achieved in previous searches.

2 CMS detector

The central feature of the CMS apparatus is a superconducting solenoid of 6 m internal diameter, providing a magnetic field of 3.8 T. Within the superconducting solenoid volume are a silicon pixel and strip tracker, a lead tungstate crystal electromagnetic calorimeter, and a brass/scintillator hadron calorimeter, each composed of a barrel and two endcap sections. In addition to the barrel and endcap detectors, CMS has extensive forward calorimetry. Muons are detected by four layers of gas-ionization detectors embedded in the steel flux-return yoke. The inner tracker measures charged particle trajectories within the pseudorapidity range $|\eta| < 2.5$. A two-stage trigger system selects pp collision events of interest for use in physics analyses. A more detailed description of the CMS detector, together with a definition of the coordinate system used and the relevant kinematic variables, can be found in Ref. [23].

3 Event reconstruction

The CMS experiment uses a particle-flow-based event reconstruction [24, 25], which aggregates information from all subdetectors. This includes charged particle tracks from the tracking system and deposited energy from the electromagnetic and hadronic calorimeters, taking advantage of excellent granularity of all sub-systems. All particle candidates are classified into

[1] Unless otherwise indicated, the symbol Z' is used in the following to refer to the resonance decaying to $t\bar{t}$, irrespective of the specific model.

muons, electrons, photons, charged hadrons, and neutral hadrons. The missing transverse momentum in the event, $E_{\mathrm{T}}^{\mathrm{miss}}$, is calculated as the imbalance in the transverse momentum of all particle flow objects. Primary vertices are reconstructed using a deterministic annealing filter algorithm [26]. The leading hard-scattering vertex of the event is defined as the vertex whose tracks have the largest squared-sum of transverse momentum.

Electrons are reconstructed in the pseudorapidity range $|\eta|$ <2.5, by combining tracking information with energy deposits in the electromagnetic calorimeter [27, 28]. Muons are detected and measured in the pseudorapidity range $|\eta|$ <2.4 using the information collected in the muon chambers and the tracking detectors [29]. Since the top-quark decay products can be collimated at high transverse momenta of the top quark, no isolation requirements on the leptons are imposed in either the trigger or offline selections.

Reconstructed particle flow candidates are clustered into jets using the FastJet 3.0 software package [30]. However, charged hadrons associated with the non-leading primary event vertex are removed prior to jet clustering. All jets are required to satisfy $|\eta| < 2.4$. The dilepton and lepton+jets analyses use jets obtained by the anti-k_{T} jet-clustering algorithm [31] with a radius parameter of 0.5 (AK5 jets). If a muon or electron is found within $\Delta R < 0.5$ of an AK5 jet, its four-momentum is subtracted from that of the jet. Jets are identified as originating from the fragmentation of a b quark by the combined secondary vertex algorithm (CSV). The loose and medium working points are used, which are defined through a misidentification probability of 10% and 1% for light-parton jets to be tagged in $\mathrm{t\bar{t}}$ events [32].

In the all-hadronic channel the Cambridge/Aachen (CA) jet-clustering algorithm [33, 34] is used, with radius parameters of 0.8 (CA8 jets) and 1.5 (CA15 jets) for the analyses at high and low values of the $\mathrm{t\bar{t}}$ invariant mass $M_{\mathrm{t\bar{t}}}$, respectively. CA8 jets are also employed in the lepton+jets analysis to identify the hadronic decay of top quarks with high p_{T} in the hemisphere separated from the lepton.

The structure of CA jets is used to distinguish hadronically decaying top quarks merged into a single jet from light quark or gluon jets, referred to as t tagging. For CA8 jets the CMS t tagging algorithm is used [35, 36], which is based on an algorithm studied in Ref. [37]. Only CA8 jets with a transverse momentum $p_{\mathrm{T}} > 400\,\mathrm{GeV}$ are considered, as at lower momenta the decay products of the hadronically decaying top quark are rarely merged into a single jet. For each CA8 jet to be t-tagged, the N-subjettiness [38, 39] ratio $\tau_{32} \equiv \tau_3/\tau_2$ is required to be smaller than 0.7.

The HEPTopTagger [40] algorithm is applied to CA15 jets. The larger radius parameter allows the identification of hadronic decays of top quarks with intermediate transverse momenta with $p_{\mathrm{T}} > 200\,\mathrm{GeV}$ [36]. Jets identified by the HEPTopTagger are called CA15 t-tagged jets henceforth.

In the all-hadronic channel, additional discriminating power against background processes is obtained from the application of the CSV algorithm to the subjets of the CA jets. A CA jet is considered to be b-tagged if the subjet with the highest discriminator value satisfies the requirement for the medium working point [32]. In the following, this algorithm will be called subjet b tagging [41].

4 Trigger and datasets

Dilepton events were collected with single lepton triggers. In particular, eμ and $\mu\mu$ events were recorded with triggers requiring a single non-isolated muon with $p_{\mathrm{T}}^{\mu} > 40\,\mathrm{GeV}$ and $|\eta| < 2.1$.

Events for the ee channel were selected using an electron trigger with a p_T threshold of 80 GeV.

The data used in the lepton+jets channel also relied on single lepton triggers. The trigger for muon events is the same one used in the dilepton analysis. The trigger for electron events required one electron with $p_T^e > 35$ GeV in conjunction with two jets that have $p_T > 100$ and 25 GeV. In both cases, no isolation requirement is applied to the leptons. A 10% increase in the signal efficiency at $M_{Z'} = 2$ TeV is gained in the electron channel by including events that were triggered by a single jet with $p_T > 320$ GeV. The events recovered by the single jet trigger contain an electron merged in a jet, which could not be resolved at the trigger level.

The all-hadronic data sample is based on two different triggers. The first requires the scalar sum of the transverse momenta of jets to be greater than 750 GeV. The second requires four jets with $p_T > 50$ GeV at trigger level, used to gain efficiency in the low mass regime with $M_{Z'} < 1$ TeV.

The $Z' \to t\bar{t}$ process is simulated using the MADGRAPH 4.4 [42] event generator, which produces a generic high mass resonance with the same left- and right-handed couplings to fermions as the SM Z boson. Higher-order parton radiations are calculated for up to three extra partons at tree-level. The simulation is performed for masses $M_{Z'}$ of 1 TeV, 1.25 TeV, 1.5 TeV, 2 TeV and 3 TeV and for decay widths of 1% and 10%. Kaluza-Klein gluon excitations are simulated using PYTHIA 8 [43]. The widths of the g_{KK} signals are about 15-20% of the resonance mass.

Top-quark events, produced via the strong and electroweak interactions, are simulated using the next-to-leading-order generator POWHEG [44]. The $W(\to \ell\nu)$+jets and $Z/\gamma^*(\to \ell\ell)$+jets processes are simulated using MADGRAPH 5.1 [45], and the diboson production processes WW, WZ and ZZ are simulated using PYTHIA 6.2 [46].

All of the samples produced with MADGRAPH are interfaced to PYTHIA for parton showering and fragmentation. The MLM algorithm [47] is applied during the parton matching to avoid double counting of partons. The MADGRAPH samples use the CTEQ6L [48] parton distribution function (PDF). For the POWHEG $t\bar{t}$ sample, the CT10 [49] PDF set is utilized, whereas the single top processes are produced with the CTEQ6M PDF. The PYTHIA Z2* tune [50] is used to characterize the underlying event.

The leading order (LO) cross sections for the Z' signal are taken from Ref. [7], whereas for g_{KK} production, calculations from Ref. [15] are used. However, both cross sections are multiplied by a factor of 1.3 [51] to approximate next-to-leading order (NLO) effects. The normalizations of the background samples are taken from the NLO+next-to-next-to leading logarithms (NNLL) calculation for the single top production [52], the next-to-next-to leading order (NNLO) calculations for $W(\to \ell\nu)$+jets and $Z/\gamma^*(\to \ell\ell)$+jets [53–55] and the NLO calculation for diboson production [56]. The normalization for the continuum $t\bar{t}$ background uses NNLO calculations [57]. However, by comparing the simulation events with data in control regions, we determine additional cross-section scale factors. This is discussed in Section 5.

5 $t\bar{t}$ event reconstruction

5.1 Dilepton channel

In the dilepton channel, the selection is based on the assumption that both W bosons from the decay of the top quark decay leptonically. The selection requires two leptons and at least two jets. The lepton and the b quark from the decay of a highly boosted top quark are usually not well separated, resulting in a non-isolated lepton that partially or fully overlaps with the b

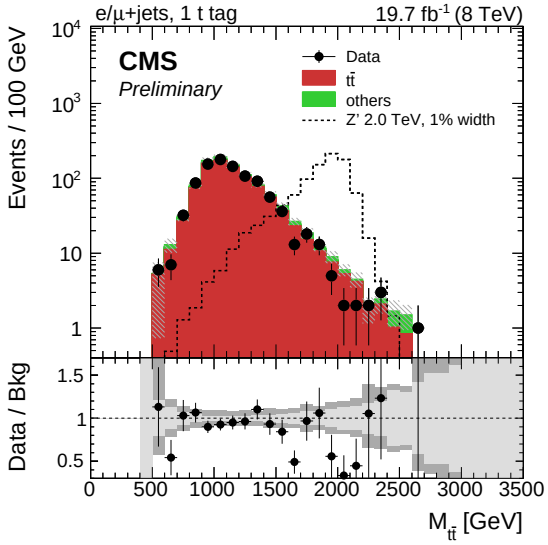

Figure 1: Invariant mass of the reconstructed $\mathrm{t\bar{t}}$ pair in data and simulation in the lepton+jets channel. Events with one CA8 t-tagged jet are shown. Each background process is scaled by a factor derived from the maximum likelihood fit to data as explained in Sec. 7, the signals are normalized to a cross section of 1 pb. The uncertainty associated with the background expectation includes all statistical and systematic uncertainties. The ratio of data/background is shown below the graph. There, the statistical uncertainty is shown in light gray, while the total uncertainty is shown in dark gray, obtained by adding the statistical and systematic uncertainties in quadrature. The expected distribution from a Z′ signal with $M_{Z'} = 2\,\mathrm{TeV}$ is also shown.

quark jet.

The analysis of the dilepton channel is described in detail in Ref. [58]. The distributions of the reconstructed $M_{\mathrm{t\bar{t}}}$ are measured in the ee, eμ and $\mu\mu$ channels. Good agreement between the data and the SM background expectation is found with no indication of additional $\mathrm{t\bar{t}}$ resonant production.

5.2 Lepton+jets channel

The selection in the lepton+jets channel is based on events with one W boson decaying leptonically, $\mathrm{W} \to \ell\nu$, and the other one decaying hadronically, $\mathrm{W} \to \mathrm{q\bar{q}}$. It requires one lepton (electron or muon) and at least two jets with high p_{T}, including events with non-isolated leptons and merged jets arising from decays of high p_{T}-top quarks.

The analysis is based on the selection and methods described in Ref. [59]. It has been extended by adding t tagging which improves the sensitivity of the analysis.

Events are categorized based on the lepton flavor and on the number of CA8 t-tagged jets. In case no CA8 t-tagged jet is found, the events are further split into two categories, depending if one or more jets are identified as originating from the fragmentation of a b quark using the medium working point of the CSV algorithm with a per-jet tagging efficiency of 65% [32]. In total six $M_{\mathrm{t\bar{t}}}$ distributions are measured, three for each lepton+jets channel. The distribution of $M_{\mathrm{t\bar{t}}}$ obtained in the lepton+jets channel is shown for events with one CA8 t-tagged jet in Fig. 1.

To validate the mistag rate of CA8 t-tagged jets in the W+jets sample, which is the dominant background in this channel before tagging, an exclusive control sample is used consisting dom-

inantely of events from W+jets production. In each event, the highest-p_T jet is used to determine the mistag rate of the CA8 t-tagged jets in data and simulated events that also contain a lepton. Such events have a higher fraction of jets from quark fragmentation than the non-top multijet background for the all-hadronic channel, which has a higher fraction of jets from gluon fragmentation. Good agreement is observed, with a mistag rate of 1.2% in data, and a ratio of data to simulation of 0.83 ± 0.21. This factor is used to scale simulated events containing a misidentified top-quark jet.

The CA8 t-tagging efficiency is extracted *in situ* by a combined maximum likelihood fit by comparing the yields in categories of events which pass and fail the CA8 t-tagging selection criteria, as explained in Sec. 7.

5.3 All-hadronic channel

When the top quark is highly boosted and the top quark decays hadronically, all decay products frequently merge into a single jet. Events with high $\mathrm{t\bar{t}}$ invariant mass, where both quarks decay hadronically, thus effectively result in a dijet topology. This forms the basis of the selection in the all-hadronic channel. The analysis in this channel is an extension of the one described in Ref. [60]. Two exclusive selections are made, one optimized for higher resonance masses, and one optimized for lower resonance masses where the decay products are less collimated.

To satisfy the high mass selection, events are required to have two CA8 t-tagged jets with $p_T > 400\,\mathrm{GeV}$ and rapidity $|y| < 2.4$. The two jets have to be separated in azimuthal angle by $|\Delta\phi| > 2.1$. The rapidity difference between the two leading jets is also used to divide the events into two categories ($|\Delta y| < 1.0$ and $|\Delta y| > 1.0$), since the QCD multijet background with light quark and gluon final states dominantly populates the $|\Delta y| > 1.0$ category, whereas the Z' signal at ~ 2 TeV is equally split between the two. The two categories are further subdivided depending on the number of subjet b-tagged CA8 jets: zero, one or two. This results in six exclusive search regions, with the highest sensitivity in the categories with two b-tagged CA8 jets.

The low mass selection is applied to events failing the high mass selection and is designed to gain sensitivity in regions where the decay products are less collimated. Events are selected if two CA15 t-tagged jets with $p_T > 200\,\mathrm{GeV}$ and $|y| < 2.4$ are found. The sample is split into events with $H_T < 800\,\mathrm{GeV}$ and $H_T > 800\,\mathrm{GeV}$, where H_T is defined as the scalar sum of jet p_T, including all jets with $p_T > 50\,\mathrm{GeV}$. The sample is further categorized according to the number of b-tagged CA15 jets.

In order to estimate the non-top multijet background, a data-driven approach is employed. A sideband is selected by inverting the CA8 t-tagging minimum mass requirement on one of the jets in the dijet sample. For the low mass analysis the CA15 t-tagging selection criteria based on the subjet invariant mass and pairwise masses are inverted. The other jet provides a kinematically-unbiased ensemble of non-top jets to measure the mistag rate. This mistag rate is then applied to the events where exactly one jet passes the t-tagging selection.

The distribution of $M_{\mathrm{t\bar{t}}}$ obtained with the low mass selection in the all-hadronic channel is shown in Fig. 2(a) for events with two subjet b tags and $H_T > 800\,\mathrm{GeV}$. The result of the high mass selection is shown in Fig. 2(b) for events with $|\Delta y| < 1.0$ and two subjet b tags. The $\mathrm{t\bar{t}}$ background process is scaled by a factor derived from the maximum likelihood fit to data as explained in Sec. 7, and the non-top multijet background is obtained from data in a sideband region.

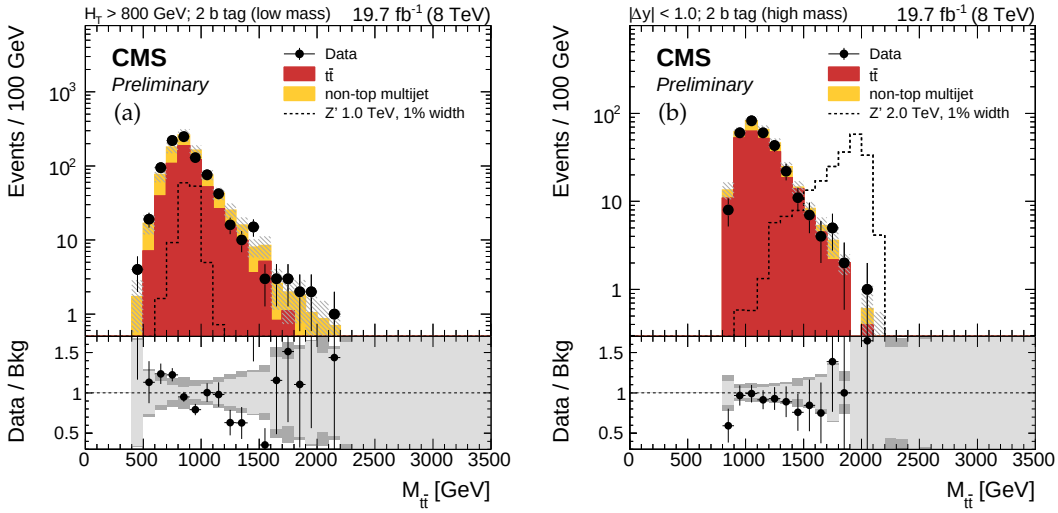

Figure 2: Reconstructed invariant mass of the $t\bar{t}$ pair in the all-hadronic channel for data and simulated events. Events are shown for the high mass selection with two t-tagged CA8 jets (a) and the low mass selection with two t-tagged CA15 jets (b). All events have two subjet b-tags. The signal is normalized to a cross section of 1 pb. The uncertainty associated with the background expectation includes all the statistical and systematic uncertainties. The ratio of data/background is shown below the distribution. There, the statistical uncertainty is shown in light gray, while the total uncertainty is shown in dark gray, obtained by adding the statistical and systematic uncertainties in quadrature. The expected distributions from a Z′ signal with $M_{Z'} = 1$ TeV and 2 TeV are also shown.

6 Systematic uncertainties

The uncertainties considered in these analyses can affect the normalization, the shape, or both normalization and shape of the $M_{t\bar{t}}$ distribution. Uncertainties originating from the same source are assumed to be 100% correlated between all channels. The dominant uncertainties are listed below.

6.1 Uncertainties affecting the normalization

The following systematic uncertainties on the normalization of the background processes are considered. The uncertainty on the cross section for $t\bar{t}$ production with $M_{t\bar{t}} > 1$ TeV is 15% [61]. Uncertainties on the production cross sections of W+jets are 9% for light flavor jets [62], and 23% for heavy flavor jets [63]. An uncertainty of 50% is assigned to the cross section of Z+jets production, obtained by varying the renormalization and factorization scales by factors of 0.5 and 2 in the calculation. The largest background contribution from single top production originates from the tW-channel, which has been measured with an accuracy of 23% [64]; this uncertainty is used for all processes with a single top quark in the final state. The uncertainty on diboson production is 20% [65, 66].

6.2 Uncertainties affecting the shape

Uncertainties on the jet energy scale and resolution are of the order of a few percent as a function of jet p_T and η. These are taken into account in all channels. Simulated events are reweighted such that the number of true pileup interactions in simulation matches the instantaneous luminosity profile in data. The systematic uncertainty associated to this reweighting is treated as fully correlated among all channels and is evaluated by varying the minimum bias cross section.

Efficiencies and mistag rates of the b-tagging algorithm have been measured in collision data and simulated events for jets [32] and subjets with a spatial separation between them of $\Delta R > 0.3$ [41]. The corresponding uncertainty is correlated between the dilepton, lepton+jets and the low mass category of the all-hadronic channel. The high mass selection in the all-hadronic channel uses subjet b tagging in a collimated region where the subjets are separated by $\Delta R < 0.3$ and the applicability of the standard b-tagging correction factors and uncertainties is not guaranteed. To account for this, the corresponding efficiency is measured simultaneously with the cross section limits *in situ*, where the efficiency is left unconstrained in the maximum likelihood fit. This corresponds to an infinite uncertainty on this variable and allows for a consistent extraction directly from the signal regions. The same procedure is used for the efficiency of the CA8 t-tagging algorithm, combined with the requirement on τ_{32}.

An uncertainty of 25% is used for mistagged CA8 t-tagged jets in simulated events, which has been studied in a side-band region of the lepton+jets channel.

In addition to the experimental uncertainties, the following uncertainties affecting the predictions of the SM background processes are considered. The effect due to missing higher orders in the simulation of SM processes is estimated by variations of the renormalization and factorization scales. The scale variations are studied in simulated W+jets and $\mathrm{t\bar{t}}$ samples, generated with scales varied by factors of two and one half. The resulting uncertainty on continuum SM $\mathrm{t\bar{t}}$ production affects all channels, while uncertainty on W+jets production only contributes to the lepton+jets channel. The effect due to the uncertainty on extra hard parton radiation is studied by varying the jet matching threshold for simulated W+jets processes by factors of two and one half. This uncertainty applies to the lepton+jets channel only. All simulated signal and background events are reweighted according to the uncertainties parameterized by the eigenvectors of CTEQ6L and CT10 PDF sets. The shifts produced by the individual eigenvectors are added in quadrature in each bin of the $M_{\mathrm{t\bar{t}}}$ distribution. The resulting uncertainty is taken to be fully correlated among all channels.

7 Background evaluation

Several SM processes contribute with different rates to the selected events. The main source of irreducible background in all channels arises from SM $\mathrm{t\bar{t}}$ production. In the lepton+jets channels, W+jets production contributes to events without a CA8 t-tagged jet. Diboson, Z+jets and single top quark production constitute small backgrounds overall, and contribute to the dilepton and lepton+jets channels. These processes are combined as "other backgrounds".

Except for the non-top multijet backgrounds in the all-hadronic channels, all SM backgrounds are estimated from simulation. Simulated samples are corrected for known differences between data and simulation and have been validated in exclusive control regions. The normalization of the simulated samples is obtained with a binned maximum likelihood fit to the reconstructed $M_{\mathrm{t\bar{t}}}$ distributions. Since there is no control sample of highly-boosted SM $\mathrm{t\bar{t}}$ events that is disjoint from the signal regions of this analysis, the maximum likelihood fit is used to extract the efficiency of the CA8 t-tagging and subject b-tagging algorithms *in situ*. This is accomplished by separating the sample into subsamples based on the tagging criteria, allowing the fit to use this information to constrain the efficiencies simultaneously with the normalization of the simulated samples. Higher order calculations, as listed in Sec. 4, are used as prior assumptions on the cross sections of each background process, with the uncertainties discussed in Sec. 6. No assumption on the scale factor for the CA8 t-tagged jets is made and the corresponding nuisance parameter is left to float freely in the fit. The same is true for the subjet b-tagging scale factor for the high mass selection in the all-hadronic channel. This procedure constrains the

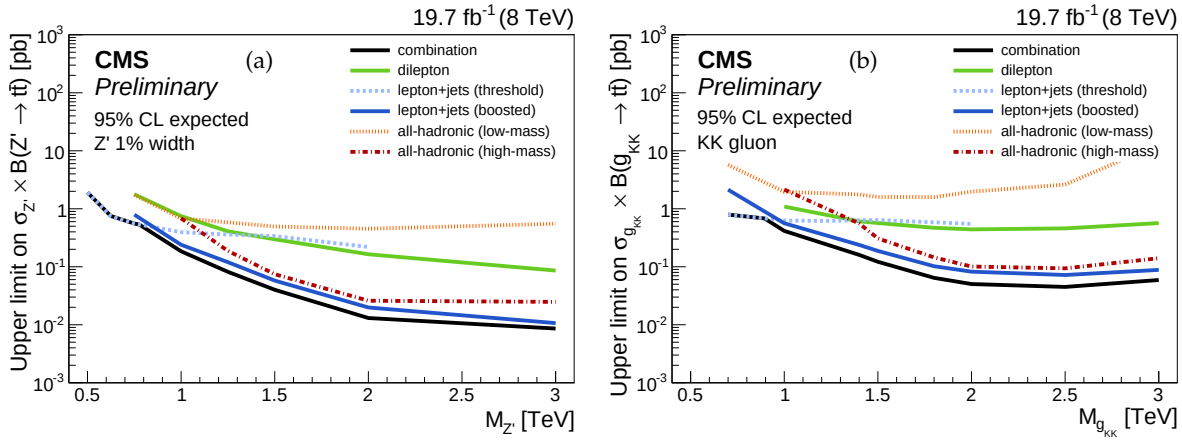

Figure 3: Expected 95% CL Bayesian upper limits on the production cross section times branching fraction for a Z′ boson decaying to $t\bar{t}$ with 1% width (a) and a KK gluon in the RS model (b). The limits obtained from the individual channels are shown separately, together with the result from the combination. Also shown are results from a threshold analysis in the lepton+jets channel [22], optimized for low masses.

tagging efficiencies effectively. The resulting uncertainties are 3% for the t-tagging scale factor, and between 3-10% for the subjet b-tagging scale factor, depending on the b-tag category.

8 Results

No significant excess of data over the expected SM background is observed. A Bayesian statistical method [67, 68] is used to derive the 95% confidence level (CL) upper limits on the cross section times branching fraction of $Z' \to t\bar{t}$ production. The limits are derived employing a template-based evaluation which uses the invariant mass distribution of the reconstructed $t\bar{t}$ pair. Correlations between the systematic uncertainties across all channels are taken into account (see Sec 6). The statistical uncertainties of simulated samples are treated as an additional Poisson nuisance parameter on each bin of the mass distribution, which is fluctuated independently.

Upper limits for three benchmark signal hypotheses are calculated: a topcolor leptophobic Z′ boson [7] with relative widths $\Gamma_{Z'}/M_{Z'} = 1.2\%$, and $\Gamma_{Z'}/M_{Z'} = 10\%$, and a Randall-Sundrum (RS) KK gluon [15]. All limits are given at 95% CL.

A comparison of the expected limits obtained from the individual channels is shown in Fig. 3. Also shown are the results from a search optimized for threshold production of the $t\bar{t}$ pair in the lepton+jets channel [22, 59]. This channel has the best sensitivity at resonance masses below 0.75 TeV. Above this value, the combination of the four boosted analyses places stronger limits on the production cross section times branching fraction. The highest overall sensitivity is obtained in the lepton+jets channel. The high mass selection of the all-hadronic channel has comparable sensitivity starting from 1.5 TeV. The dilepton and low mass all-hadronic channels contribute mostly in the region of 0.75–1 TeV to the combined limits.

Figure 4 shows the results for each of the three signal hypotheses. The cross section limits for the narrow signal hypothesis are compared to the cross section for the production of a Z′ boson with 1.2% width. This specific width is chosen to compare to theoretical results and previous

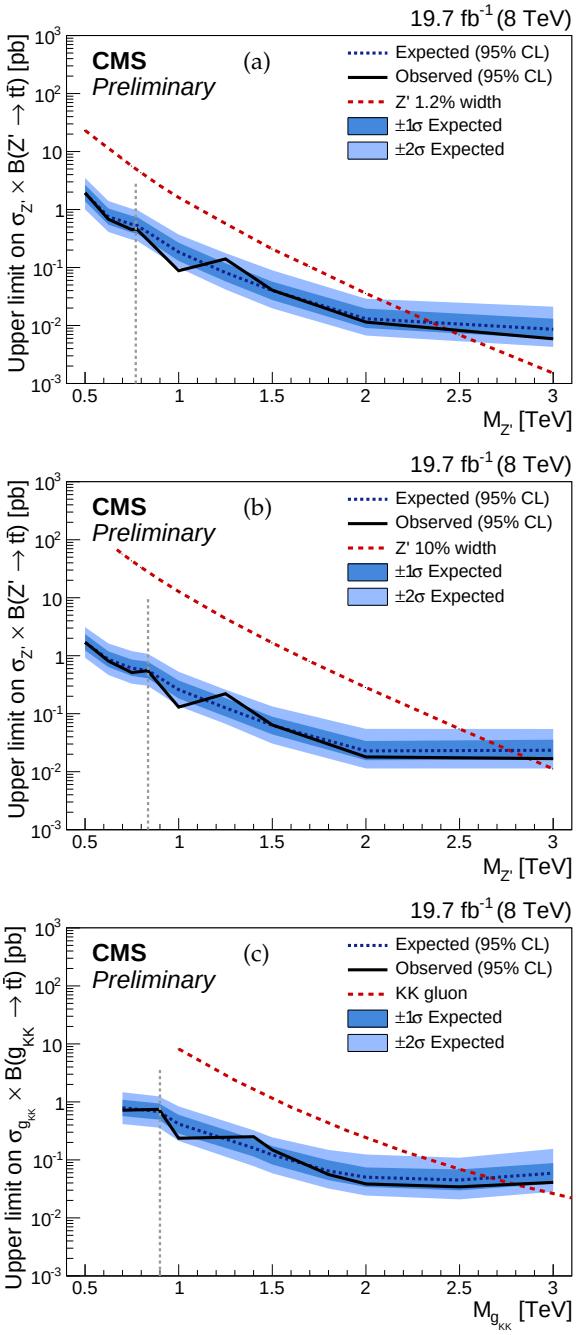

Figure 4: 95% CL bayesian upper limits on the production cross section times branching fraction for a Z′ boson decaying to $t\bar{t}$ with 1% width (a), with 10% width (b) and a KK gluon in the Randall–Sundrum model decaying to $t\bar{t}$ (c). The vertical dashed line indicates the transition from a threshold analysis [22] to the combination, in providing the best expected limit. Below this dashed line, only the results of the low mass analysis with resolved jets are quoted; above this line, the results from the combination of the boosted channels are given. The limits are shown as a function of the resonance mass and are compared to predictions for the cross section of a Z′ boson with relative width of 1.2% and 10% [7] and the prediction for the production of a KK gluon [15]. The predictions are multiplied by a factor of 1.3 to account for higher-order corrections [51].

Table 1: Observed and expected lower mass limits for the three benchmark models. Mass limits are given for the dilepton analysis, the lepton+jets analysis, the combination of the two all-hadronic analyses and the full combination of all four analyses. All limits are given at 95% CL.

signal hypothesis	mass limit [TeV]							
	dilepton channel		lepton+jets channel		all-hadronic channels		**combined**	
	obs.	exp.	obs.	exp.	obs.	exp.	obs.	exp.
Z', $\Gamma_{Z'}/M_{Z'} = 1.2\%$	1.5	1.4	2.3	2.2	2.1	2.1	**2.4**	**2.4**
Z', $\Gamma_{Z'}/M_{Z'} = 10\%$	2.2	2.1	2.8	2.7	2.5	2.5	**2.9**	**2.8**
RS KK gluon	2.0	1.8	2.5	2.5	2.3	2.4	**2.8**	**2.7**

measurements. Resonances with masses up to 2.4 TeV (2.4 TeV expected) for the narrow Z′ hypothesis are excluded at 95% CL. These cross section limits are model independent, meaning that they are valid for any resonance decaying to $\mathrm{t\bar{t}}$, with a width well below the experimental resolution of about 10%. Wide resonances with 10% width are excluded up to 2.9 TeV (2.8 TeV expected). The better limits with respect to narrow resonances are due to the higher production cross section of the wider Z′ resonance. RS KK gluons decaying to $\mathrm{t\bar{t}}$ are excluded with masses below 2.8 TeV (2.7 TeV expected). This model exhibits the weakest upper limits on the production cross section, because of the long tails towards low resonance masses present in the predicted $M_{\mathrm{t\bar{t}}}$ distribution. These tails are introduced by the interplay between the large natural width of the KK gluons and the parton luminosity, causing masses that are far below the resonance mass to have a larger probability than events near the resonance itself. The expected and observed exclusion limits for different resonance masses are given in Table 1.

The upper limits on the cross sections show improvements of about 50% with respect to a previous combination of results from a search in the lepton+jets and all-hadronic channels [22]. These improvements are mostly due to the usage of t tagging in the lepton+jets channel, and the application of b tagging on subjets in the all-hadronic channel. The limits at $M_{Z'} < 1$ TeV are improved with the addition of the dilepton channel and the low mass selection in the all-hadronic channel.

9 Summary

A search has been performed for the production of heavy $\mathrm{t\bar{t}}$ resonances in final states including two, one or no leptons. The analysis is based on the data sample corresponding to an integrated luminosity of 19.7 fb^{-1} recorded in 2012 by the CMS detector in pp collisions at $\sqrt{s} = 8$ TeV at the LHC. No evidence is found for a resonant $\mathrm{t\bar{t}}$ component beyond the standard model $\mathrm{t\bar{t}}$ continuum production. Model-independent cross section limits are set on the production of such resonances with a width well below the experimental resolution of about 10%.

The obtained mass limits improve upon previous ones set at $\sqrt{s} = 7$ TeV [17, 20, 21] by several hundreds of GeV. An improvement by about 50% on the 95% CL upper limits on the cross section with respect to a previous search optimized for high masses at $\sqrt{s} = 8$ TeV [22] is achieved by the application of additional jet substructure information and the addition of the dilepton channel.

References

[1] CMS Collaboration, "Observation of a new boson at a mass of 125 GeV with the CMS experiment at the LHC", *Phys. Lett. B* **716** (2012) 30, doi:10.1016/j.physletb.2012.08.021, arXiv:1207.7235.

[2] ATLAS Collaboration, "Observation of a new particle in the search for the Standard Model Higgs boson with the ATLAS detector at the LHC", *Phys. Lett. B* **716** (2012) 1, doi:10.1016/j.physletb.2012.08.020, arXiv:1207.7214.

[3] CMS Collaboration, "Observation of a new boson with mass near 125 GeV in pp collisions at $\sqrt{s} = 7$ and 8 TeV", *JHEP* **06** (2013) 081, doi:10.1007/JHEP06(2013)081, arXiv:1303.4571.

[4] C. Hill, "Topcolor: Top quark condensation in a gauge extension of the standard model", *Phys. Lett. B* **266** (1991) 419, doi:10.1016/0370-2693(91)91061-Y.

[5] C. Hill and S. Parke, "Top production: Sensitivity to new physics", *Phys. Rev. D* **49** (1994) 4454, doi:10.1103/PhysRevD.49.4454, arXiv:hep-ph/9312324.

[6] C. Hill, "Topcolor Assisted Technicolor", *Phys. Lett. B* **345** (1995) 483, doi:10.1016/0370-2693(94)01660-5, arXiv:hep-ph/9411426. Updates in arXiv:hep-ph/9911288.

[7] R. M. Harris and S. Jain, "Cross sections for leptophobic topcolor Z' decaying to top-antitop", *Eur. Phys. J. C* **72** (2012) 2072, doi:10.1140/epjc/s10052-012-2072-4, arXiv:1112.4928.

[8] J. Rosner, "Prominent decay modes of a leptophobic Z'", *Phys. Lett. B* **387** (1996) 113, doi:10.1016/0370-2693(96)01022-2, arXiv:hep-ph/9607207.

[9] K. Lynch et al., "Finding Z-prime bosons coupled preferentially to the third family at LEP and the Tevatron", *Phys. Rev. D* **63** (2001) 035006, doi:10.1103/PhysRevD.63.035006, arXiv:hep-ph/0007286.

[10] M. Carena et al., "Z-prime gauge bosons at the Tevatron", *Phys. Rev. D* **70** (2004) 093009, doi:10.1103/PhysRevD.70.093009, arXiv:hep-ph/0408098.

[11] P. Frampton and S. Glashow, "Chiral color: An alternative to the standard model", *Phys. Lett. B* **190** (1987) 157, doi:10.1016/0370-2693(87)90859-8.

[12] D. Choudhury et al., "Top production at the Tevatron/LHC and nonstandard, strongly interacting spin one particles", *Phys. Lett. B* **657** (2007) 69, doi:10.1016/j.physletb.2007.09.057, arXiv:0705.1499. Updates in arXiv:0810.3635.

[13] D. Dicus, A. Stange, and S. Willenbrock, "Higgs decay to top quarks at hadron colliders", *Phys. Lett. B* **333** (1994) 126, doi:10.1016/0370-2693(94)91017-0, arXiv:hep-ph/9404359.

[14] L. Randall and R. Sundrum, "A Large mass hierarchy from a small extra dimension", *Phys. Rev. Lett.* **83** (1999) 3370, doi:10.1103/PhysRevLett.83.3370, arXiv:hep-ph/9905221.

[15] K. Agashe et al., "LHC Signals from Warped Extra Dimensions", *Phys. Rev. D* **77** (2008) 015003, doi:10.1103/PhysRevD.77.015003, arXiv:hep-ph/0612015.

[16] H. Davoudiasl, J. Hewett, and T. Rizzo, "Phenomenology of the Randall-Sundrum Gauge Hierarchy Model", *Phys. Rev. Lett.* **84** (2000) 2080, doi:10.1103/PhysRevLett.84.2080, arXiv:hep-ph/9909255.

[17] CMS Collaboration, "Search for anomalous $\mathrm{t\bar{t}}$ production in the highly-boosted all-hadronic final state", *JHEP* **09** (2012) 029, doi:10.1007/JHEP09(2012)029, arXiv:1204.2488.

[18] ATLAS Collaboration, "A search for $\mathrm{t\bar{t}}$ resonances in lepton+jets events with highly boosted top quarks collected in pp collisions at $\sqrt{s}$= 7 TeV with the ATLAS detector", *JHEP* **09** (2012) 041, doi:10.1007/JHEP09(2012)041, arXiv:1207.2409.

[19] ATLAS Collaboration, "Search for $\mathrm{t\bar{t}}$ resonances in the lepton plus jets final state with ATLAS using 4.7 fb^{-1} of pp collisions at $\sqrt{(s)}$ = 7 TeV", *Phys. Rev. D.* **88** (2013) 012004, doi:10.1103/PhysRevD.88.012004, arXiv:1305.2756.

[20] CMS Collaboration, "Search for resonant $t\bar{t}$ production in lepton+jets events in pp collisions at $\sqrt{s} = 7$ TeV", *JHEP* **12** (2012) 015, doi:10.1007/JHEP12(2012)015, arXiv:1209.4397.

[21] CMS Collaboration, "Search for Z′ resonances decaying to $\mathrm{t\bar{t}}$ in dilepton+jets final states in pp collisions at $\sqrt{s}$ = 7 TeV", *Phys. Rev. D* **87** (2013) 072002, doi:10.1103/PhysRevD.87.072002, arXiv:1211.3338.

[22] CMS Collaboration, "Searches for new physics using the $t\bar{t}$ invariant mass distribution in pp collisions at $\sqrt{s}$=8 TeV", *Phys. Rev. Lett.* **111** (2013) 211804, doi:10.1103/PhysRevLett.111.211804, arXiv:1309.2030.

[23] CMS Collaboration, "The CMS experiment at the CERN LHC", *JINST* **3** (2008) S08004, doi:10.1088/1748-0221/3/08/S08004.

[24] CMS Collaboration, "Particle–Flow Event Reconstruction in CMS and Performance for Jets, Taus, and $E_{\mathrm{T}}^{\mathrm{miss}}$", CMS Physics Analysis Summary CMS-PAS-PFT-09-001, 2009.

[25] CMS Collaboration, "Commissioning of the Particle-flow Event Reconstruction with the first LHC collisions recorded in the CMS detector", CMS Physics Analysis Summary CMS-PAS-PFT-10-001, 2010.

[26] A. Aimar, J. Harvey, and N. Knoors, eds., "Deterministic Annealing for Vertex Finding at CMS", number CERN-2005-002. CERN, Geneva, (2005). doi:10.5170/CERN-2005-002.

[27] CMS Collaboration, "Performance of electron reconstruction and selection with the CMS detector in proton-proton collisions at sqrt(s)=8 TeV", arXiv:1502.02701. CMS-EGM-13-001.

[28] CMS Collaboration, "Energy Calibration and Resolution of the CMS Electromagnetic Calorimeter in pp Collisions at $\sqrt{s} = 7$ TeV", *JINST* **8** (2013) P09009, doi:10.1088/1748-0221/8/09/P09009, arXiv:1306.2016.

[29] CMS Collaboration, "Performance of CMS muon reconstruction in pp collision events at $\sqrt{s} = 7$ TeV", *JINST* **7** (2012) P10002, doi:10.1088/1748-0221/7/10/P10002, arXiv:1206.4071.

[30] M. Cacciari, G. P. Salam, and G. Soyez, "FastJet user manual", *Eur. Phys. J. C* **72** (2012) 1896, doi:10.1140/epjc/s10052-012-1896-2, arXiv:1111.6097.

[31] M. Cacciari, G. P. Salam, and G. Soyez, "The anti-k_t jet clustering algorithm", *JHEP* **04** (2008) 063, doi:10.1088/1126-6708/2008/04/063, arXiv:0802.1189.

[32] CMS Collaboration, "Identification of b-quark jets with the CMS experiment", *JINST* **8** (2013) P04013, doi:10.1088/1748-0221/8/04/P04013, arXiv:1211.4462.

[33] Y. L. Dokshitzer, G. D. Leder, S. Moretti, and B. R. Webber, "Better jet clustering algorithms", *JHEP* **08** (1997) 001, doi:10.1088/1126-6708/1997/08/001, arXiv:hep-ph/9707323.

[34] M. Wobisch and T. Wengler, "Hadronization corrections to jet cross sections in deep-inelastic scattering", (1999). arXiv:hep-ph/9907280. DESY-PROC 1999-02.

[35] CMS Collaboration, "A Cambridge-Aachen (C-A) based Jet Algorithm for boosted top-jet tagging", CMS Physics Analysis Summary CMS-PAS-JME-09-001, 2009.

[36] CMS Collaboration, "Boosted Top Jet Tagging at CMS", CMS Physics Analysis Summary CMS-PAS-JME-13-007, 2014.

[37] D. E. Kaplan, K. Rehermann, M. D. Schwartz, and B. Tweedie, "Top Tagging: A Method for Identifying Boosted Hadronically Decaying Top Quarks", *Phys. Rev. Lett.* **101** (2008) 142001, doi:10.1103/PhysRevLett.101.142001, arXiv:0806.0848.

[38] J. Thaler and K. Van Tilburg, "Identifying Boosted Objects with N-subjettiness", *JHEP* **1103** (2011) 015, doi:10.1007/JHEP03(2011)015, arXiv:1011.2268.

[39] J. Thaler and K. Van Tilburg, "Maximizing Boosted Top Identification by Minimizing N-subjettiness", *JHEP* **1202** (2012) 093, doi:10.1007/JHEP02(2012)093, arXiv:1108.2701.

[40] T. Plehn, M. Spannowsky, M. Takeuchi, and D. Zerwas, "Stop Reconstruction with Tagged Tops", *JHEP* **1010** (2010) 078, doi:10.1007/JHEP10(2010)078, arXiv:1006.2833.

[41] CMS Collaboration, "Performance of b tagging at $\sqrt{s}$ = 8 TeV in multijet, ttbar and boosted topology events", CMS Physics Analysis Summary CMS-PAS-BTV-13-001, 2013.

[42] J. Alwall et al., "MadGraph/MadEvent v4: The New Web Generation", *JHEP* **0709** (2007) 028, doi:10.1088/1126-6708/2007/09/028, arXiv:0706.2334.

[43] S. T., M. S., and S. P., "A Brief Introduction to PYTHIA 8.1", *Comput. Phys. Commun.* **178** (2008) doi:10.1016/j.cpc.2008.01.036, arXiv:0710.3820.

[44] S. Alioli, P. Nason, C. Oleari, and E. Re, "A general framework for implementing NLO calculations in shower Monte Carlo programs: the POWHEG BOX", *JHEP* **06** (2010) 043, doi:10.1007/JHEP06(2010)043, arXiv:1002.2581.

[45] J. Alwall et al., "MadGraph 5 : Going Beyond", *JHEP* **06** (2011) 128, doi:10.1007/JHEP06(2011)128, arXiv:1106.0522.

[46] S. T., M. S., and S. P., "PYTHIA 6.4 Physics and Manual", *JHEP* **0605** (2006) 026, doi:10.1088/1126-6708/2006/05/026, arXiv:0603175.

[47] M. L. Mangano, M. Moretti, F. Piccinini, and M. Treccani, "Matching Matrix Elements and Shower Evolution for Top-Quark Production in Hadronic Collisions", *JHEP* **01** (2007) 013, doi:10.1088/1126-6708/2007/01/013, arXiv:0611129.

[48] P. M. Nadolsky et al., "Implications of CTEQ global analysis for collider observables", *Phys. Rev. D* **78** (2008) 013004, doi:10.1103/PhysRevD.78.013004, arXiv:0802.0007.

[49] H.-L. Lai et al., "New parton distributions for collider physics", *Phys. Rev. D* **82** (2010) 074024, doi:10.1103/PhysRevD.82.074024, arXiv:1007.2241.

[50] R. Field, "Min-bias and the underlying event at the LHC", *Acta Physica Polonica B* **42** (2011) 2631, doi:doi:10.5506/APhysPolB.42.2631.

[51] J. Gao, C. S. Li, B. H. Li, and H. X. Zhu, "Next-to-leading order QCD corrections to a heavy resonance production and decay into top quark pair at the LHC", *Phys. Rev. D* **82** (2010) 014020, doi:10.1103/PhysRevD.82.014020, arXiv:1004.0876.

[52] N. Kidonakis, "NNLL threshold resummation for top-pair and single-top production", *Phys. Part. Nucl.* **45** (2014) 714, doi:10.1134/S1063779614040091, arXiv:1210.7813.

[53] R. Gavin, Y. Li, F. Petriello, and S. Quackenbush, "FEWZ 2.0: A code for hadronic Z production at next-to-next-to-leading order", *Comput. Phys. Commun.* **182** (2011) 2388, doi:10.1016/j.cpc.2011.06.008, arXiv:1011.3540.

[54] R. Gavin, Y. Li, F. Petriello, and S. Quackenbush, "W Physics at the LHC with FEWZ 2.1", *Comput. Phys. Commun.* **184** (2013) 208, doi:10.1016/j.cpc.2012.09.005, arXiv:1201.5896.

[55] Y. Li and F. Petriello, "Combining QCD and electroweak corrections to dilepton production in FEWZ", *Phys. Rev.* **D86** (2012) 094034, doi:10.1103/PhysRevD.86.094034, arXiv:1208.5967.

[56] J. Campbell, R. Ellis, and K. Williams, "Vector boson pair production at the LHC", *JHEP* **07** (2011) 018, doi:10.1007/JHEP07(2011)018, arXiv:1105.0020.

[57] M. Czakon, P. Fiedler, and A. Mitov, "Total Top-Quark Pair-Production Cross Section at Hadron Colliders Through $O(\alpha_s^4)$", *Phys. Rev. Lett.* **110** (2013) 252004, doi:10.1103/PhysRevLett.110.252004, arXiv:1303.6254.

[58] CMS Collaboration, "Search for ttbar resonances in dilepton+jets final states in pp collisions at 8 TeV", CMS Physics Analysis Summary CMS-PAS-B2G-12-007, CERN, Geneva, 2014.

[59] CMS Collaboration, "Search for ttbar resonances in semileptonic final state", CMS Physics Analysis Summary CMS-PAS-B2G-12-006, CERN, Geneva, 2013.

[60] CMS Collaboration, "Search for Anomalous Top Quark Pair Production in the Boosted All-Hadronic Final State using pp Collisions at sqrt(s) = 8 TeV", CMS Physics Analysis Summary CMS-PAS-B2G-12-005, CERN, Geneva, 2013.

[61] CMS Collaboration, "Measurement of the differential $t\bar{t}$ cross section in the dilepton channel at 8 TeV", CMS Physics Analysis Summary CMS-PAS-TOP-12-028, CERN, Geneva, 2013.

[62] CMS Collaboration, "Differential cross section measurements for the production of a W boson in association with jets in protonproton collisions at $\sqrt{s} = 7$ TeV", *Phys. Lett.* **B741** (2015) 12, doi:10.1016/j.physletb.2014.12.003, arXiv:1406.7533.

[63] CMS Collaboration, "Measurement of the production cross section for a W boson and two b jets in pp collisions at $\sqrt{s}$=7 TeV", *Phys. Lett.* **B735** (2014) 204, doi:10.1016/j.physletb.2014.06.041, arXiv:1312.6608.

[64] CMS Collaboration, "Observation of the associated production of a single top quark and a W boson in pp collisions at $\sqrt{s}$ = 8 TeV", *Phys. Rev. Lett.* **112** (2014) 231802, doi:10.1103/PhysRevLett.112.231802, arXiv:1401.2942.

[65] CMS Collaboration, "Measurement of W^+W^- and ZZ production cross sections in pp collisions at $\sqrt{s}$ = 8 TeV", *Phys. Lett.* **B721** (2013) 190, doi:10.1016/j.physletb.2013.03.027, arXiv:1301.4698.

[66] CMS Collaboration, "Measurement of WZ and ZZ production in pp collisions at $\sqrt{s} = 8$ TeV in final states with b-tagged jets", *Eur. Phys. J.* **C74** (2014) 2973, doi:10.1140/epjc/s10052-014-2973-5, arXiv:1403.3047.

[67] A. O'Hagan and J. J. Forster, "Kendalls Advanced Theory of Statistics. Vol. 2B: Bayesian Inference". Arnold, London, 2004.

[68] J. Ott. http://www.theta-framework.org.